Shape from Diffuse Polarisation

Gary Atkinson and Edwin Hancock
Department of Computer Science
University of York, York, YO1 5DD, UK.
atkinson@cs.york.ac.uk

Abstract

When unpolarised light is reflected from a smooth dielectric surface, it is spontaneously partially polarised. This process applies to both specular and diffuse reflection, although the effect is greatest for specular reflection. This paper is concerned with exploiting this phenomenon by processing images of smooth dielectric objects to recover surface normals and hence height. The paper presents the underlying physics of polarisation by reflection, starting with the Fresnel equations. It is explained how these equations can be used to obtain the shape of objects and some experimental results are presented to illustrate the usefulness of the theory.

1 Introduction

Polarisation has proved to be a useful source of information in the analysis of light scattering from surfaces in computer vision. There are a number of ways in which polarisation arises and can be used in surface analysis. Perhaps the most familiar example is when the incident light is polarised and the polarisation of the scattered light is analysed [8]. When the scattering process is coherent, then the polarisation of the incident light is preserved, whereas polarisation is destroyed when the scattering process is incoherent. This property can be used to remove specularities from surfaces. However, there are more subtle polarisation effects that can be exploited. For instance, under certain conditions initially unpolarised light becomes polarised as a result of the reflection [16]. This applies to both specular reflection (which we refer to as specular polarisation) and diffuse reflection (diffuse polarisation) and is due to the directionality of the molecular electron charge density interacting with the electromagnetic field of the incident light [3].

There is a considerable amount of literature on the use of polarisation for surface analysis. Most research aimed at extracting and interpreting information from polarisation data, involves placing a linear polarizer in front of a camera and taking images of an object or a scene with the polarizer oriented at different angles [16, 6]. Recently however, liquid crystal technology has enabled more rapid acquisition of polarization images at a rate such that several complete sets of polarisation data can be obtained per second [15]. The polarisation cameras that have been developed are particularly useful for outdoor scenes and scenes involving moving objects for practical reasons. For controlled laboratory conditions however, the older method is still of use.

Note that most of this work relies on specular polarisation and controlled lighting conditions. In some previous work [11, 5] the object under investigation was placed inside a spherical diffuser, with several light sources outside and a hole for the camera.

BMVC 2004 doi:10.5244/C.18.94

With this set up, specular reflection occurs across the whole of the object and, since specular reflection is generally much stronger than diffuse reflection, the latter component can be ignored. Other research has focused on separating diffuse and specular reflection components using colour [13, 7], a probabilistic framework [8] or polarisation [16, 14]. The relevant theory can then be applied to the specular or diffuse images. This existing work has demonstrated the usefulness of polarisation in surface height recovery, image segmentation and recognition and separation of reflection components.

In contrast to the bulk of previous work, the aim of this paper is to investigate the extent to which spontaneously acquired *diffuse* polarisation can be used to recover surface geometry. In particular, we aim to explore how it can be used to estimate surface orientation near the limbs of shiny objects. To do this we make use of Fresnel Theory, which relates the reflected and incident wave amplitudes and provides a route to estimating the surface normals from polarisation data. The angle of maximum transmission through a polaroid filter together with the range of measured brightness can be used to make estimates of the azimuth and zenith angles of the surface normals. This leads to an algorithm that uses three measured intensities to estimate the surface normal direction. We experiment with the method on real world data, and this demonstrates that measurements of diffuse polarisation can be used to make relatively accurate surface normal estimates, and that these surface normal estimates can be used for realistic surface height recovery.

2 Polarisation and Reflection

In this section, some of the key physics of reflection from smooth surfaces is discussed, with particular emphasis on how measurements of the polarisation state of reflected light can be used in computer vision. It is assumed that the incident light is unpolarised.

The electric field of an electromagnetic wave incident on a surface causes electrons of the reflecting medium near the surface to vibrate. These vibrating electrons re-radiate, generating the reflected rays. For electric fields perpendicular to the plane of incidence (which is defined as the plane that contains the normal vector of the surface at a specularly reflecting point and the vectors pointing from that point to both the light source and the detector) the electrons also vibrate perpendicular to the plane and, thus so does the electric field of the reflected light. For light polarised parallel to the plane of incidence on the other hand, the electrons do not vibrate perpendicularly to the reflected ray, as Fig. 1 shows, resulting in a more attenuated wave. The effect is particularly marked for smooth surfaces composed of microfacets, as significant roughness tends to depolarise the light. As Fig. 1 suggests, the degree of polarisation depends on the angle of incidence. Later, we show how this description can be extended, by considering internal scattering, to account for partial polarisation of diffusely reflected light.

2.1 Review of Fresnel Coefficients for Dielectrics

The Fresnel equations give the ratios of reflected wave amplitude to incident wave amplitude for incident light that is linearly polarised perpendicular to, or parallel to, the plane of specular incidence [1]. These ratios depend upon the angle of incidence and the refractive index of the reflecting medium. Since the incident light can be always be resolved into components perpendicular to, and parallel to, the plane of incidence, the Fresnel equations are applicable to all incident polarisation states.

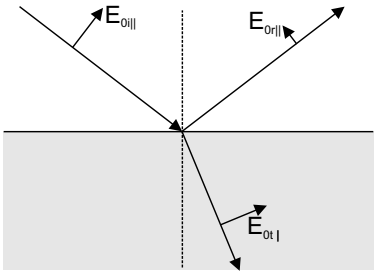

Figure 1: Reflection of a wave polarised parallel to the plane of incidence. Within the medium, the electrons vibrate parallel to the electric field. Since this direction is not perpendicular to the reflected wave, only a component of the vibrations cause a reflected ray.

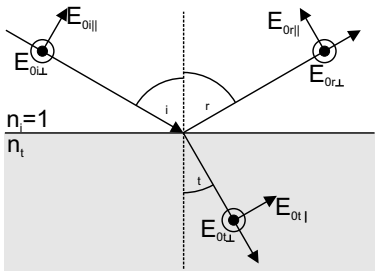

Figure 2: Definitions. Directions of electric fields are indicated. N.B. $\theta_i = \theta_r$.

For the geometry of Fig. 2, and assuming that the material is non-magnetic, the amplitude reflection coefficients for perpendicularly polarised light, $r_\perp$, and parallel polarised light, $r_\parallel$, at a boundary between two media are given by

$$r_\perp \equiv \frac{E_{0r\perp}}{E_{0i\perp}} = \frac{n_i \cos\theta_i - n_t \cos\theta_t}{n_i \cos\theta_i + n_t \cos\theta_t}, \qquad r_\parallel \equiv \frac{E_{0r\parallel}}{E_{0i\parallel}} = \frac{n_t \cos\theta_i - n_i \cos\theta_t}{n_t \cos\theta_i + n_i \cos\theta_t} \tag{1}$$

where n_i and n_t are the refractive indices of the first and second media and θ_i and θ_t are incident and transmitted angles. θ_t can be obtained from the well-known Snell's Law:

$$n_i \sin\theta_i = n_t \sin\theta_t \tag{2}$$

Generally, it is not the amplitude of the wave that is measured by the detector, but the intensity, which is proportional to the square of the amplitude. With this in mind, it is possible to show [1] that the *intensity coefficients* are $R_\perp = r_\perp^2$ and $R_\parallel = r_\parallel^2$. All this assumes that the refractive index is wavelength independent [2]. In fact, there is some wavelength dependence, but the equations above provide reasonable results for many situations.

Figure 3a shows the Fresnel intensity coefficients for a typical dielectric. At about 60° (typical for most dielectrics) the parallel component of reflected light is zero. This angle is known as the *Brewster* or *polarising* angle. The figure suggests that there is some information contained in the polarisation state of reflected light, as for specular reflection more of the light polarised perpendicularly to the plane of incidence is reflected than that parallel to the plane. This means that the reflected light is *partially linearly polarised*, that is, the light is comprised of an unpolarised component, and a completely polarised component.

2.2 The Polarisation Image

We now consider how the above theory can be used in computer vision. As a polarizer placed in front of the camera is rotated, the measured intensity varies sinusoidally. From Fig. 3, it is clear that the maximum and minimum intensities detected for a particular surface orientation are

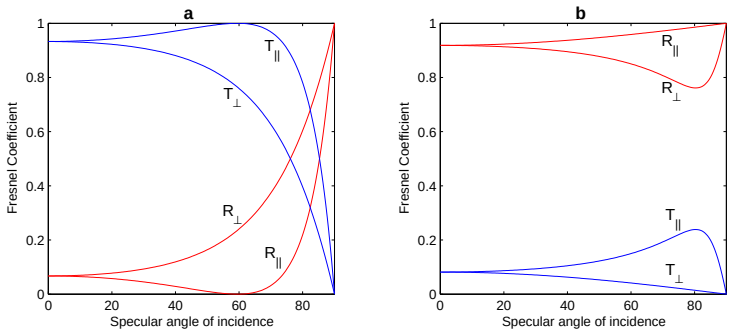

Figure 3: (a) Reflection and transmission coefficients for a dielectric ($n = 1.7$). For comparison (b) shows the coefficients for a metal ($n = 0.8$, $k = 6$, where k is the extinction coefficient [1]. Note that n can be less than one if $k > 0$. For dielectrics, $k = 0$ and the equations presented in this paper assume that this is the case).

$$I_{\max} = \frac{R_\perp}{R_\perp + R_\parallel} I_s \; ; \quad I_{\min} = \frac{R_\parallel}{R_\perp + R_\parallel} I_s \tag{3}$$

where I_s is the magnitude of the specular component of reflection (assume for now, that there is no diffuse reflection). The *degree of polarisation* or *partial polarisation*, which is frequently used in computer vision, is defined by

$$\rho = \frac{I_{\max} - I_{\min}}{I_{\max} + I_{\min}} \tag{4}$$

Each polarisation image, i.e. the full set of polarisation data for a given object or scene, is comprised of three separate images. The first of these is the *intensity image*, which is simply the image that would be obtained using a normal camera.

Secondly, there is the *phase image* where the intensity encodes the orientation of the polarizer corresponding to maximum transmission through it. The phase is therefore the angle of the linearly polarised component of reflected light. Note that the polarizer cannot distinguish between x and $x + 180^\circ$, so the range of initially acquired phase measurements is $[0, 180^\circ)$. There is therefore a 180° ambiguity, since two maxima in intensity are found as the polarizer is rotated through 360°. Possible methods for dealing with this problem include pointing the estimates away from the object at the occluding boundary, and propagating into the object [6], tracing level curves [9] or applying some form of optimisation algorithm possibly involving smoothing (which would have the added benefit of reducing effects of noise but results in loss of sharp edges).

The final part of the polarisation image is the degree of polarisation, as determined by (4). One way to obtain this is to take many images over a large number of polarizer orientations; indeed this method is less susceptible to noise. However, taking three images and fitting the data to a sine wave usually suffices and needs fewer images.

[15] suggests taking three images I_0, I_{45} and I_{90} corresponding to polarizer orientations of 0°, 45° and 90° respectively, and using the following to determine the phase (5), intensity (6) and degree of polarisation (7):

$$\phi = \frac{1}{2}\arctan\left(\frac{I_0 + I_{90} - 2I_{45}}{I_{90} - I_0}\right) + 90^\circ$$

$$\text{if}\,(I_{90} < I_0)\,[\text{if}\,(I_{45} < I_0)\,\phi = \phi + 90^\circ \text{else} \phi = \phi - 90^\circ] \tag{5}$$

$$I = I_0 + I_{90} \tag{6}$$

$$\rho = \frac{I_{90} - I_0}{(I_{90} + I_0)\cos 2\phi} \tag{7}$$

2.3 Shape from Specular Polarisation

Following the dichromatic reflectance model [12], the reflected light is a superposition of specular and diffuse components. Specular reflection is a result of direct surface reflection and is the only component for metals. As Fig. 3a shows, the reflected light is attenuated more if it is polarised parallel to the specular plane. Thus, greatest transmission through the polarizer occurs when the polarizer is oriented at an angle 90° from the *azimuth* angle of the surface. Orthographic projection is assumed.

The zenith angle, the angle which the normal makes with the viewing direction, can be computed by considering the degree of polarisation. Substituting (3) into (4) gives the degree of specular polarisation in terms of the Fresnel coefficients:

$$\rho_s = \frac{R_\perp(n,\theta_i) - R_\parallel(n,\theta_i)}{R_\perp(n,\theta_i) + R_\parallel(n,\theta_i)} \tag{8}$$

Using (8) with the Fresnel equations gives ρ in terms of n and the zenith angle, θ. Unfortunately, n is not generally known, but for most dielectrics is approximately 1.7 and dependence of ρ_s on n is weak. Thus, with a known value or estimate of n, and with ρ_s measured using (4), θ can be determined.

Fig. 4a shows the dependence of ρ_s on θ. Note that at the Brewster angle $\rho_s = 1$ since the light is totally polarised[1]. Also, there is a 2-to-1 mapping of ρ_s to θ, resulting in another ambiguity that must be solved [5].

2.4 Shape from Diffuse Polarisation

The degree of diffuse polarisation is highest, and so most useful, near occluding edges where the zenith angle is large. Diffuse polarisation has the advantage that less controlled lighting conditions are required than for specular polarisation but disadvantages that it is not applicable to metals and transparent objects and is more susceptible to noise.

Diffuse polarisation is a result of the following process [16]: A portion of the incident light penetrates the surface, is partially polarised in the process and is internally refracted. Due to the random nature of internal scattering, the light gets depolarised. Some of the light is then refracted back into the air and is, once again, refracted and partially polarised.

[1] In practice ρ_s will be a little less than 1 due to a small, but finite, diffuse component of reflection.

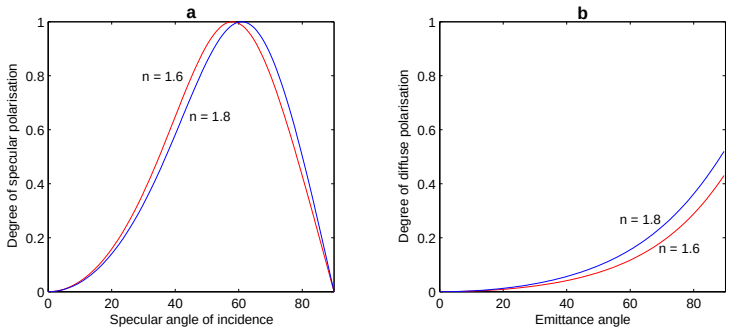

Figure 4: Degree of polarisation for (a) specular and (b) diffuse reflection for two different refractive indices. Most opaque dielectrics have refractive indices between these two values

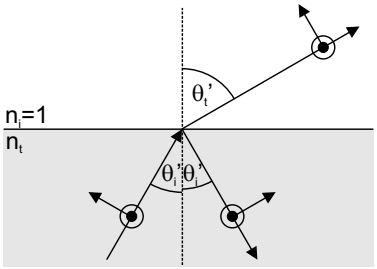

Figure 5: Transmission of internally scattered light back into air.

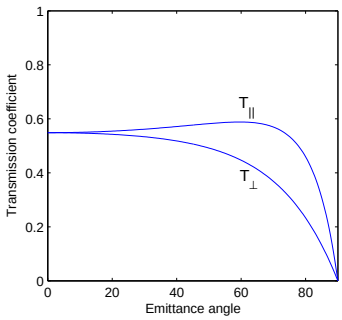

Figure 6: Fresnel coefficients for Fig. 5 ($n = 1.7$).

When light approaches the interface from within the medium, as shown in Fig. 5, a similar process to that discussed earlier takes place but with the relative index of refraction being $1/n$ instead of n (assuming refractive index of air = 1). If the internal angle of incidence is above a critical angle ($\arcsin 1/n$), then total internal reflection occurs. Otherwise, Snells Law (2) can be used to find the angle of emittance for any given angle of internal incidence. The Fresnel transmission coefficient[2] can then be calculated for a given *emittance* angle. Fig. 6 shows the result of this calculation for a typical dielectric with an additional factor of $1/n$ introduced due to a difference in wave impedance. It should be pointed out that diffuse polarisation also results from multiple scattering from microfacets, to which this theory clearly cannot be applied, although this contribution is small for smooth surfaces.

Using (4), the degree of diffuse polarisation is

$$\rho_d = \frac{T_\parallel(1/n,\theta_i') - T_\perp(1/n,\theta_i')}{T_\parallel(1/n,\theta_i') + T_\perp(1/n,\theta_i')} = \frac{R_\perp(1/n,\theta_i') - R_\parallel(1/n,\theta_i')}{2 - R_\perp(1/n,\theta_i') - R_\parallel(1/n,\theta_i')} \tag{9}$$

Snell's Law (2) can be used to interchange between internal angle of incidence, and the

[2]The transmission coefficients are simply $T_\perp = 1 - R_\perp$ and $T_\parallel = 1 - R_\parallel$

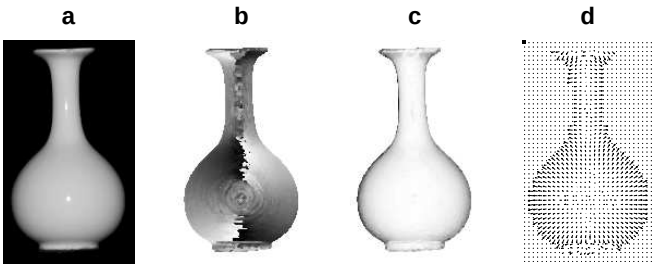

Figure 7: (a) Greyscale image of porcelain vase. (b) Measured phase. The circle of constant phase at the centre of the bulb is a result of the smoothing algorithm used to reduce noise. (c) Degree of polarisation. Dark areas have highest polarisation. (d) Needle map (low resolution).

more useful angle of emittance. Fig. 4b shows the degree of diffuse polarisation for different angles using the resulting equation:

$$\rho_d = \frac{(n-1/n)^2 \sin^2\theta}{2-2n^2-(n+1/n)^2\sin^2\theta+4\cos\theta\sqrt{n^2-\sin^2\theta}} \tag{10}$$

The zenith angle can be found from (10). The azimuth angle can be determined using exactly the same method as the one used for specular reflection, except that a phase shift of 90° is necessary. The need for a phase shift is illustrated by Fig. 6, which shows that light of parallel polarisation has a higher transmission coefficient and so greater intensity is associated with a polarizer at that orientation. This is in contrast to specular reflection (Fig. 3).

3 Experimental Results

As (5) – (7) show, three images, with the polarizer oriented at 0°, 45° and 90°, are sufficient to obtain the phase and degree of polarisation of a scene. Images were therefore taken, with a linear polarizer placed in front of a camera at these angles, of smooth porcelain objects. In principle, the results should not be critically dependent upon lighting conditions as it is only the orientation of the surface and its index of refraction that determines the polarisation state of the reflected light. To simplify matters however, only one light source was used, placed behind the camera so that specularities occurred only at points on the surface where the zenith angle was zero. The camera was an Olympus E-10 digital SLR. The walls of the room and the table on which the objects lay were black so that pixels of the images having an intensity below a certain threshold could be treated as background. Fig. 7 shows the result of the phase and degree of polarisation computation.

The phase image was then converted into azimuth vectors by taking the sine and cosine at each pixel. At this stage the 180° ambiguity is still present. The degree of polarisation is converted to zenith angle by numerically solving (10). It is assumed throughout this work that the refractive index of the reflecting medium is 1.7. After normalising the vectors so they were unit length and applying the disambiguation routine outlined below, the needle map shown in Fig. 7d was obtained.

Throughout this work, the camera was set up such that the diffusely reflected light intensity varies across the whole dynamic range of the camera. A noise reduction technique

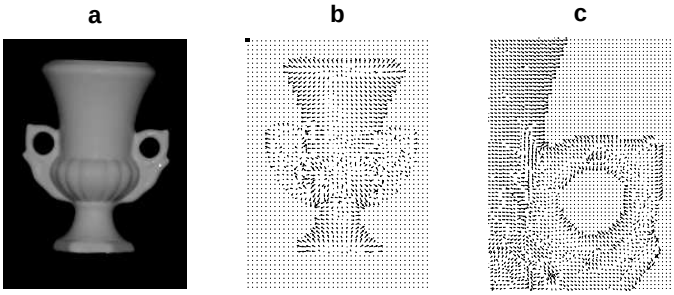

Figure 8: Needle map of a porcelain urn. The close-up shows that details are picked up reasonably well. The calculated phase to the left of the handle in (c) is 90° from the expected values. This is due to a specular interreflection and will be the focus of future work.

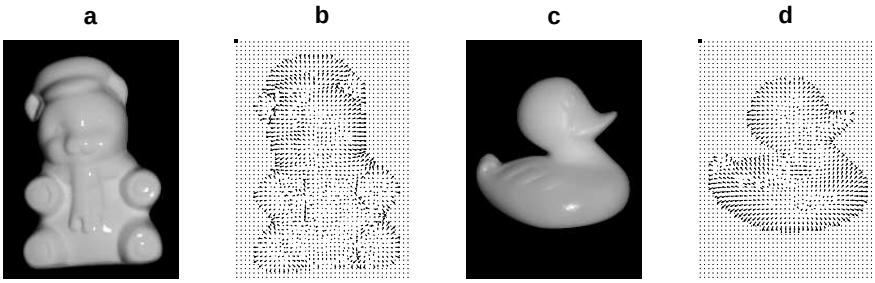

Figure 9: (a) Application of the algorithm to a porcelain bear. This clearly illustrates the main strength of the technique, with the normals accurately acquired near occluding edges, and weakness, with some details missing at small zenith angles. (b) Application to a slightly rough plastic duck, showing that the applicability of the technique is not restricted to *perfectly* smooth objects.

that we used involved processing pixels by taking median intensities over local neighbourhoods, with central pixels being counted more than once, giving them extra "weighting." This was improved by smoothing over larger neighbourhoods for areas of higher degree of polarisation. We later implemented an adaptive smoothing algorithm, which was used to obtain Figs. 7–9 [4]. We found that, without adaptive smoothing, it was often necessary to take several images at each polarizer angle and use the average image at each angle.

The next step in processing the images was to disambiguate the azimuth components of surface normals. This was achieved in two different ways. Firstly a program was written to allow manual selection of regions of the image where the vectors should be rotated by 180°. A better method was then introduced that orders the pixels of the image according to zenith angle with greatest angles listed first. Since we know that the vectors at the occluding contours must be pointing outward, we can propagate into the object using the order calculated previously and assuming no abrupt changes in azimuth angle (except for small zenith angles). This method gave good results for the vase, but variable results far from the limbs for more complex objects (Figs. 8 and 9) due, in part, to insoluble convex/concave ambiguities.

The final step in processing was to recover the depth from surface normals. This was

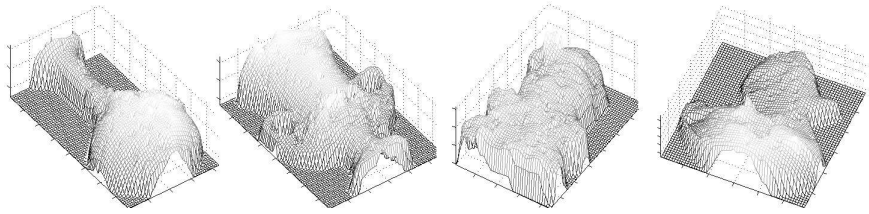

Figure 10: Depth maps of porcelain vase, urn and bear and plastic duck computed by applying the algorithm of [10] to the needle maps and rotating the objects to different angles.

performed using the algorithm reported in [10], which uses a graph-spectral method. The result of the application of this algorithm is shown in Fig. 10. It is quite clear that the basic shapes have been recovered, but with noise being problematic at small zenith angles.

4 Conclusion

This study of shape from diffuse polarisation has accomplished two tasks. Firstly it has shown that there is potential for using diffuse polarisation in geometry analysis, despite the common assumption that the difference between reflected polarisation components is negligible for diffuse reflection. Secondly however, it illustrates the fact that away from the occluding contours of complex objects, diffuse polarisation is limited in applicability. Diffuse polarisation is best used therefore, in conjunction with other techniques such as shape from shading or shape from specular polarisation.

Other limitations of shape from diffuse polarisation include the non-trivial disambiguation routine and the requirement of three images (although, as mentioned earlier, polarisation cameras are now removing this requirement). The main advantages are that the algorithms are very reliable at obtaining azimuth and zenith angles from images of smooth dielectrics close to occluding contours and that no light source information needs to be known, although the reflection must be diffuse.

There is potential for future work with diffuse polarisation from rougher surfaces. The zenith angles would be more difficult to obtain since the random microfacet orientation has a depolarising effect, reducing the degree of polarisation. This means that either more information on the microscopic surface structure would be needed, or an empirical lookup table generated from images of an object of known shape. Due to the lower degree of polarisation, noise would be more problematic, especially away from occluding contours. For metals [16] and transparent materials [5], the diffuse component of reflection is almost zero so specular reflection must be used.

References

[1] M. Born and E. Wolf. *Principles of Optics. Electromagnetic Theory of Propagation, Interference and Diffraction of Light.* Pergamon, London, 1959.

[2] R.L. Cook and K.E. Torrance. A reflectance model for computer graphics. *ACM Transactions on Computer Graphics*, 1:7–24, 1982.

[3] E. Hecht. *Optics*. Addison Wesley Longman, third edition, 1998.

[4] C. Kervrann. An adaptive window approach for image smoothing and structures preserving. In *Proc. ECCV*, volume 3, pages 132–144, 2004.

[5] D. Miyazaki, M. Kagesawa, and K. Ikeuchi. Transparent surface modelling from a pair of polarization images. *IEEE Trans. Patt. Anal. Mach. Intell.*, 26:73–82, 2004.

[6] D. Miyazaki, R.T. Tan, K. Hara, and K. Ikeuchi. Polarization-based inverse rendering from a single view. In *Proc. ICCV*, volume 2, pages 982–987, 2003.

[7] S.K. Nayar, X. Fang, and T. Boult. Separation of reflectance components using colour and polarization. *Intl. J. Computer Vision*, 21:163–186, 1997.

[8] H. Ragheb and E. Hancock. A probabilistic framework for specular shape from shading. *Pattern Recognition*, 36:407–427, 2003.

[9] S. Rahmann. Polarization images: A geometric interpretation for shape analysis. In *Proc. of ICPR*, volume 3, pages 542–546, 2000.

[10] R. Robles-Kelly and E. Hancock. A graph-spectral method for surface height recovery from needle-maps. In *Proc. of CVPR*, pages 141–148, 2001.

[11] M. Saito, Y. Sato, K. Ikeuchi, and H. Kashiwagi. Measurement of surface orientations of transparent objects using polarization in highlight. In *Proc. of CVPR*, volume 1, pages 381–386, 1999.

[12] S. Shafer. Using color to separate reflection components. *Colour Research Applications*, 10:210–218, 1985.

[13] R.T. Tan and K. Ikeuchi. Separating reflection components of textured surfaces using a single image. In *Proc. ICCV*, volume 2, pages 870–877, 2003.

[14] S. Umeyama. Separation of diffuse and specular components of surface reflection by use of polarization and statistical analysis of images. *IEEE Trans. Pattern Anal. Mach. Intell*, 26:639–647, 2004.

[15] L.B. Wolff. Polarization vision: A new sensory approach to image understanding. *Image and Vision Computing*, 15:81–93, 1997.

[16] L.B. Wolff and T.E. Boult. Constraining object features using a polarisation reflectance model. *IEEE Trans. Pattern Anal. Mach. Intell*, 13:635–657, 1991.